PHILOSOPHICAL TRANSACTIONS OF THE ROYAL SOCIETY A MATHEMATICAL, PHYSICAL & ENGINEERING SCIENCES

Stick-Slip Vibrations and Chaos

K. Popp and P. Stelter

Phil. Trans. R. Soc. Lond. A 1990 **332**, 89-105
doi: 10.1098/rsta.1990.0102

Stick–slip vibrations and chaos

By K. Popp and P. Stelter

Institute of Mechanics, University of Hannover, Appelstrasse 11, D-3000 Hannover 1, F.R.G.

Stick–slip vibrations are self-sustained oscillations induced by dry friction. They occur in engineering systems as well as in our everyday life, e.g. the sound of bowed instruments results from stick–slip vibrations of the strings. Two discrete and two continuous models of stick–slip systems have been investigated in this paper, which exhibit rich bifurcational and chaotic behaviour. Results from numerical simulations and experimental observations could be obtained. In the latter case, chaos has to be distinguished from noise in the measurements. This requires special analysis methods like the reconstruction of a pseudo-state space from a time series and the calculation of the so-called correlation integral.

1. Introduction

What do squeaking doors, stringed instruments, squealing railway wheels, grating brakes and rattling machine tools have in common? Well, they are examples of self-sustained oscillations due to dry friction (Magnus 1961). This type of oscillation is often found in our everyday life as well as in engineering systems. Recent investigations of oscillations induced by dry friction have shown that beside the well-known limit cycle behaviour, chaotic motions are also possible, depending on the system parameters (Popp & Stelter 1990; Stelter & Popp 1989).

The aim of our research is to investigate simple mechanical models under self-excitation due to dry friction, to show the transition from regular to chaotic motions and the corresponding parameter dependencies as well. Beside analytical and numerical results, some experimental observations are also presented. In the latter case, one has to distinguish between chaotic phenomena and noise in the measurements, which requires appropriate analysis methods.

Dry friction appears in two different phenomena in nature: (i) as a resistance against the beginning of a motion starting from equilibrium (stick mode); (ii) as a resistance against an existing motion (slip mode).

The friction resistance is a constraining force in the stick mode and an applied force in the slip mode. In an oscillatory motion both phenomena take place successively, resulting in a stick–slip mode. Since the friction characteristic consists of two qualitatively different parts with a non-smooth transition, the resulting motion also shows a non-smooth behaviour. Thus, stick–slip systems belong to the class of non-smooth systems, where discontinuities occur on a surface in the state space (Utkin 1978). Other examples are systems with stops, impacts, hysteresis or active systems with a discontinuous control. Furthermore, in stick–slip systems some degrees of freedom are blocked during the stick mode; thus, they also belong to the class of

Phil. Trans. R. Soc. Lond. A (1990) **332**, 89–105 *Printed in Great Britain*

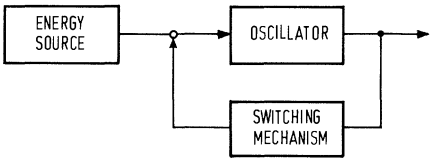

Figure 1. Block diagram of a self-sustained vibration system.

non-smooth systems with a variable structure, where the number of state variables changes with time. Further examples are systems with play or rest, e.g. snap-in mechanisms.

It is well known that non-smooth systems can exhibit chaotic behaviour. Engineering problems of this type where chaos was found numerically and/or experimentally are the following: a hinged bar with periodic impulsive loading (cf. Hsu 1987), a moored vessel bouncing against a stiff fender (cf. Thompson & Stewart 1986), impact print hammers in a matrix printer (Hendriks 1983), a vibrating beam with an amplitude constraining stop (Moon & Shaw 1983), a rotor touching a boundary (Szczygielski 1986), lateral motion of a railway bogie (Kaas-Petersen & True 1985), rattling gear drives (Pfeiffer 1988), a constrained pipe conveying fluid (Paidoussis & Moon 1988). Unfortunately, these systems cannot be analysed by methods that require certain smoothness assumptions on the nonlinear functions involved. For example, the common methods for calculating Lyapunov exponents cannot be applied. Therefore, new ways of investigation have to be found.

There exists a rich literature on chaos in self-excited systems with smooth nonlinearities (Guckenheimer & Holmes 1983; Abraham & Shaw 1983–88; Kunick & Steeb 1986; Thompson & Stewart 1986; Neimark & Landa 1987). However, in case of self-excitation due to dry friction only a few hints for chaotical behaviour can be found (Popp *et al.* 1985; Grabec 1988; Fingberg 1989).

2. The violin as an example

To become acquainted with friction-induced self-sustained oscillations, the vibration of a violin string will be considered. Each self-excited vibration system encounters an energy source, an oscillator, and a switching mechanism triggered by the oscillator, which controls the energy flow from the source to the vibrating systems (cf. figure 1). If the energy flow into the vibration system is greater (less) than the dissipation during one period, then the vibration amplitude will increase (decrease). If the energy input and output is balanced during each period, then an isolated periodic motion can be observed, which is known to be a limit cycle. Obviously, for a violin the energy source is represented by the motion of the bow and the oscillator is given by the string. Figure 2 shows a simple model of a continuous violin string and an even simpler discrete spring-mass-model which is excited by a continuous belt instead of a bow. But how is the energy transferred from the bow to the string and what is the switching mechanism? Here, the dry friction between bow and string comes into play (this is why the bow is treated with colophony). From Coulomb's friction laws, the difference between the static friction coefficient μ_0 and the kinetic friction coefficient μ is well known, where $\mu_0 > \mu$ holds. However, many

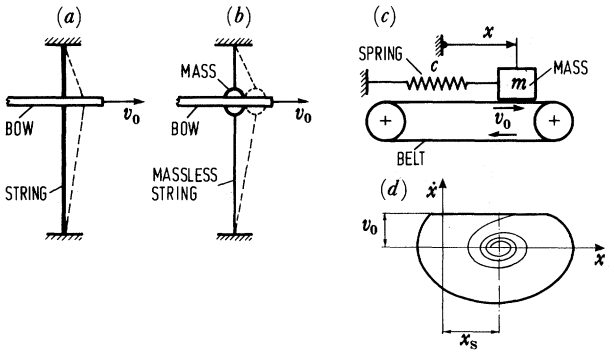

Figure 2. Simple models for a violin string: (*a*) continuous string, (*b*) massless string with a concentrated mass, (*c*) discrete spring-mass system driven by a continuous belt, (*d*) phase-plane plot.

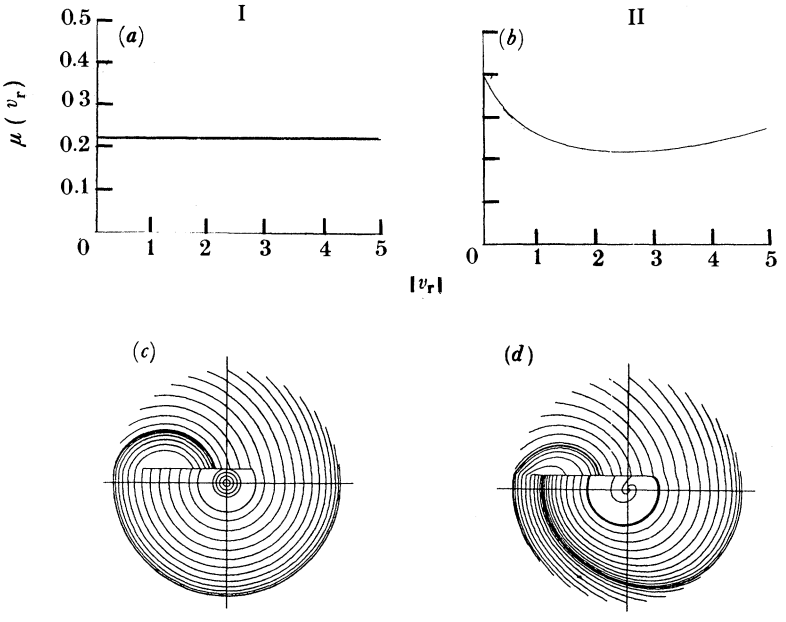

Figure 3. Friction characteristics with the corresponding phase-plane plots for the discrete violin string model (figure 2*c*). (*a*) $\mu(v_r) = \mu_0$ for $v_r = 0$, $\mu(v_r) = \mu$ for $v_r \neq 0$. (*b*) $\mu(v_r) = (\mu_0 - \mu_1)/(1 + \lambda|v_r|) + \mu_1 + \alpha v_r^2$. (*c*) $\mu_0 = 0.4$, $\mu = 0.23$. (*d*) $\mu_0 = 0.4$, $\mu = 0.1$, $\lambda = 99.4\ \mathrm{s\ m^{-1}}$, $\alpha = 0.7\ \mathrm{s^2\ m^{-2}}$.

experimental investigations proved the dependence of the kinetic friction coefficient μ on the relative velocity v_r of the rubbing surfaces, $\mu = \mu(v_r)$, where a decreasing characteristic for small values v_r was observed (Conti 1875; Galton 1878; Franke 1882; Bochet 1961). Figure 3 shows two different friction models I and II depending on two and four parameters, respectively. The corresponding stick–slip motion for the spring-mass model is visualized in the phase plane, where velocity $\dot{x}$ against displacement x of the mass is plotted. The qualitative behaviour is equal for both friction models. Although the motion of a real violin string is more complicated, the

energy transfer from the bow to the string can be explained by means of the discrete model of a spring-restrained block on a continuous belt; see figure 2 (cf. Bishop 1965). If the belt is moving, then the block will start to oscillate. This motion takes place, because the friction between the block and the belt is greater for small slipping velocities than for large ones. By starting from standstill, the velocity of the belt will be always greater than the fluctuating velocity of the block so that the direction of sliding is always equal. Hence, the friction force exerted upon the block has always the same direction which coincides with the direction of the belt motion. But while the block moves in the direction of the belt, the velocity of slip is smaller and the friction force is larger than by moving in the opposite direction. Thus a surplus of energy is transferred to the block during one cycle of motion which leads to increasing amplitudes of displacement and velocity of the block. When the block velocity reaches the band velocity, the block sticks to the band and moves with it until the restoring spring force becomes larger than the static friction force acting upon the block. Now, the limit cycle is reached, where stick–slip motions appear.

The equation of motion for the discrete model depend on the relative velocity $v_r = \dot{x} - v_0$ between block and band. For the slip mode, $v_r \neq 0$, the following equation is given:

$$m\ddot{x} + F_s = F_R(v_r), \quad F_s = cx. \tag{1}$$

The friction force $F_R(v_r)$ is an applied force,

$$F_R(v_r) = -\mu(v_r) F_N \operatorname{sgn}(v_r), \tag{2}$$

depending on the friction characteristic $\mu(v_r)$.

For the stick mode with $v_r = 0$ it follows:

$$\dot{x} = v_0, \quad \ddot{x} = 0, \quad F_R(v_r = 0) = F_s = cx. \tag{3}$$

The friction force $F_R(v_r = 0)$ is a reaction force which is constrained by the static friction law,

$$|F_R(v_r = 0)| \leqslant \mu_0 F_N, \quad \mu_0 = \mu(v_r = 0). \tag{4}$$

Here, F_N denotes the normal force, $F_N \geqslant 0$, and F_s the restoring spring force.

The main features of the stick–slip motion are the same for both friction laws, as it can be seen from figure 3. Thus, Coulomb's simple 2-parameter friction model with $\mu_0 \neq \mu$, $\mu = \mu(v_r) = \text{const.}$, will be chosen to construct the phase-plane plots, cf. figure 4:

For $v_r < 0$ from (1), (2) it follows

$$\ddot{x} + \omega_0^2 x = \mu F_N/m, \quad \omega_0^2 = c/m. \tag{5}$$

The corresponding solution reads

$$x(t) = \mu F_N/c + C\cos(\omega_0 t - \varphi), \tag{6}$$

where C and φ can be determined from the initial conditions. This solution can be characterized by circles about $(+\mu F_N/c, 0)$ in the $x, \dot{x}/\omega_0$-phase plane. Similarly, $v_r > 0$ yields circles about $(-\mu F_N/c, 0)$ in the phase plane, where $\mu F_N/c \equiv x_s$ is

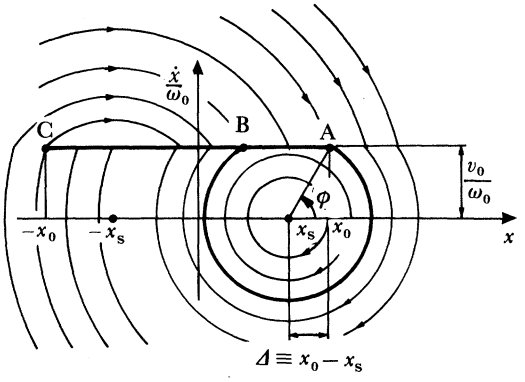

Figure 4. Phase-plane plots for the discrete violin string model with a simplified friction characteristic, cf. figure 3*a*. $x_0 = \mu_0 F_N/c$, $x_s = \mu F_N/c$.

the equilibrium position, cf. (1), (2). On the other hand, from (3), (4) the limit points x_A, x_C for the stick mode can be calculated,

$$|x| \leqslant \mu_0 F_N/c \equiv x_0, \tag{7}$$

$$x_C = -x_0 \leqslant x \leqslant +x_0 = x_A. \tag{8}$$

The advantage of this simplified model is, that the phase portrait can easily be established, see figure 4. Due to the simplified friction model where the decreasing characteristic is replaced by a discontinuity, the limit curve A–B–A is not the only periodic solution and is also not smooth in A in contrast to the limit cycles for continuous friction models, cf. figure 3. However, this simple model allows two limit cases to be deduced, where either the stick mode or the slip mode dominates during one period of the limit cycle. This is also important in the case of a violin (cf. Cremer 1981). The distance Δ, $\Delta \equiv x_0 - x_s = (\mu_0 - \mu) F_N/c$, is proportional to the difference between the maximum static and kinetic friction force. If $\Delta \ll v_0/\omega_0$ or $1/\tan\varphi \ll 1$, cf. figure 4, then the friction force will be small compared with the restoring and inertia forces. In this case the slip mode is dominant and a nearly harmonic motion results, where the frequency is close to the natural frequency $f, f \approx f_0 = \omega_0/2\pi$, of the free oscillator and the corresponding period is $T \approx T_0 = 2\pi/\omega_0$. On the other hand, if $\Delta \gg v_0/\omega_0$ or $\tan\varphi \ll 1$, then the stick mode will be dominant and the friction and restoring forces govern the motion, while the inertia forces are negligible. In this case, a sawtooth-like relaxation motion comes up, where the period is approximately $T \approx 2\Delta/v_0$ and the corresponding frequency is $f \approx v_0/2\Delta$. In the frequency spectrum of this motion, many higher harmonics appear. The motion for the two limit cases is visualized in figure 5. Therefore, the sound of a violin string will be quite different for these two limit cases.

However, the oscillations of a real violin string are much more complicated than the vibrations of the discrete spring-mass model. First of all, the violin string is a continuous oscillator, where wave propagation takes place. This has experimentally been investigated by Helmholtz with a 'vibration-microscope' (cf. Helmholtz 1913). Furthermore, the torsional motion of the string as well as its bending stiffness are of

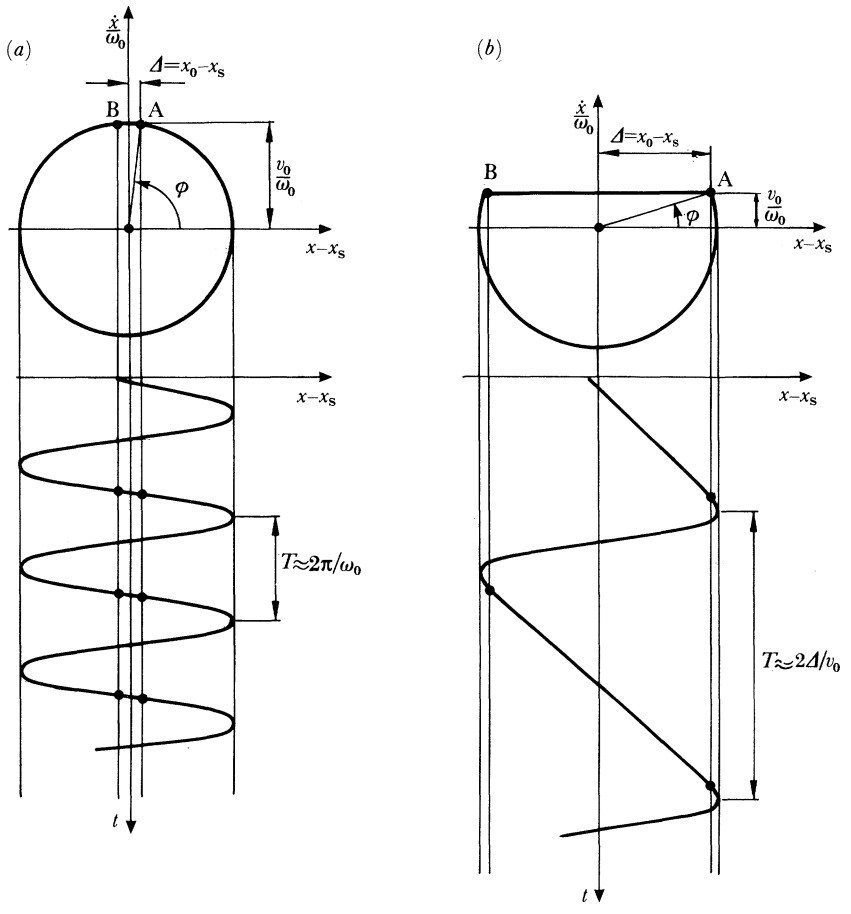

Figure 5. Limit cases of the violin motion: (*a*) harmonic motion for $\Delta \ll v_0/\omega_0$, (*b*) relaxation motion for $\Delta \gg v_0/\omega_0$.

importance (Cremer 1981). A sophisticated model for computer simulations has been developed by McIntyre & Woodhouse (1979). But, to evaluate the sound of a violin, the strings together with the sound box and the connecting parts have to be investigated. One motivation for doing this is to explain the sound quality of the violins made by the famous old Italian masters and, perhaps, to lift the secret of their craftsmanship (cf. Skalmierski 1981). But this is not the aim of the present paper. On the other hand, an interesting question is, Can a violin string oscillate in a chaotic manner? Or in other words, can a violin sound chaotically? Intuitively, to the last question an affirmative answer will be given, due to audible experiences with beginners playing the violin, cf. figure 6. However, up to now, there are no systematic investigations on chaotic oscillations of a violin string. The discrete model described by equations (1) to (4) is not complex enough to exhibit chaotic motions. But other discrete and continuous models will be shown, where rich bifurcational and chaotic phenomena occur.

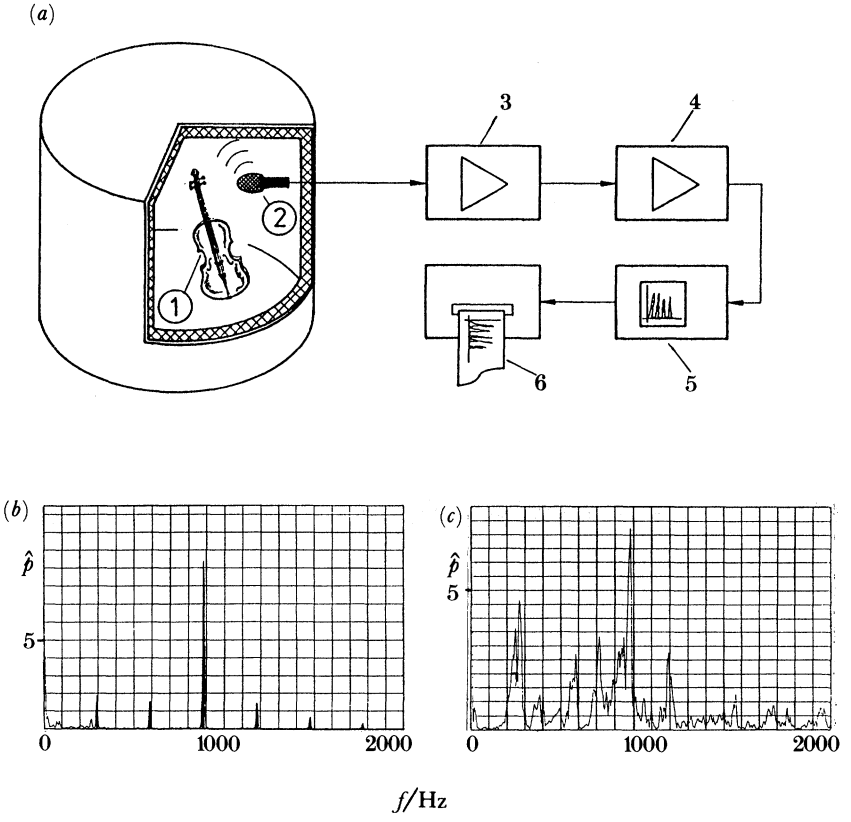

Figure 6. Measurement of the violin sound: (*a*) test set-up with violin 1 and microphone 2 in an insulated room, preamplifier 3, signal amplifier 4, FFT-analyser 5, plotter 6 with frequency plots of the measured sound pressure for (*b*) normal tone *d*, (*c*) 'chaotic' tone *d* played with large bow speed and large bow pressure.

3. Some discrete and continuous models of stick–slip system

In all systems under consideration, self-excitation is induced by the friction force of a continuous belt acting on the structure. Two discrete and two continuous models have been investigated as shown in figure 7.

The two discrete systems have been investigated numerically only. They serve as simple model problems to show different phenomena, parameter dependencies and routes to chaos. The two continuous systems have been investigated experimentally: (i) to get evidence of chaotic behaviour, (ii) to develop analysis techniques which are applicable in the presence of noise, and (iii) to gain data for comparisons with numerical results. Important questions which should be answered by means of experiments are: How to develop simple models for continuous systems being able to describe chaos? How to separate noise in the measurements from deterministic chaos?

For the numerical analysis of the discrete models, the friction characteristic (II), cf. figure 3, has been assumed with the parameters $\mu_0 = 0.4$, $\mu_1 = 0.1$, $\lambda = 1.42$ s m^{-1}, $\alpha = 0.01$ s^2 m^{-2}, if not specified otherwise.

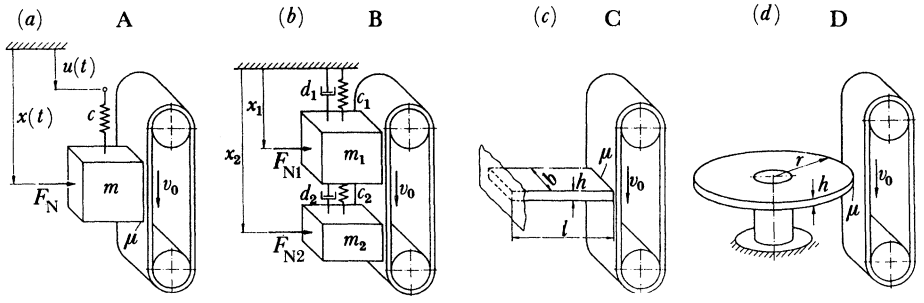

Figure 7. Discrete and continuous models of systems which show friction induced self-sustained oscillations: (*a*) single-degree-of-freedom oscillator with an external harmonic excitation, (*b*) a two-degree-of-freedom spring-mass-damper-system, (*c*) a cantilever beam as a one-dimensional continuous system, (*d*) a thin centrally fixed plate as a two-dimensional continuous system.

Model A represents a simultaneous self- and external excited vibration system. The equations of motion read in non-dimensional state space notation:

$$\left.\begin{aligned} x_1' &= x_2, \\ x_2' &= -x_1 + [F_R(-v_0) - F_R(v_r)]/c + u_0 \cos(x_3), \\ x_3' &= \eta, \end{aligned}\right\} \tag{9}$$

with the abbreviations

$$\left.\begin{aligned} (*)' = \mathrm{d}(*)/\mathrm{d}\tau, \quad \tau = \omega_0 t, \quad \omega_0 = \sqrt{(c/m)}, \quad \eta = \Omega/\omega_0, \\ x_1 \equiv \bar{x} = x - x_s, \quad v_r = \omega_0 x_2 - v_0, \quad x_s = \mu(v_0) F_N/c, \end{aligned}\right\} \tag{10}$$

where m means mass, c spring stiffness, v_0 belt velocity, u_0 excitation amplitude and Ω excitation frequency. The parameter values and initial conditions are, if not specified otherwise: $v_0 = 1.0$ m s^{-1}, $F_N/c = 10.0$ m, $u_0 = 0.5$ m, $\omega_0 = 1.0$ rad s^{-1}, $\eta = 2.1$, and $x_1(0) = 0$, $x_2(0) = 1.0$ m s^{-1}, respectively.

Similarly, for model B, which represents a two-degree-of-freedom self-sustained vibration system, we have:

$$\left.\begin{aligned} x_1' &= x_2, \\ x_2' &= \gamma^{-1}\{-(1+\kappa)x_1 - 2D(1+\delta)x_2 + x_3 + 2Dx_4 + [F_R(-v_0) - F_R(v_{r1})]/c_2\}, \\ x_3' &= x_4, \\ x_4' &= x_1 + 2Dx_2 - x_3 - 2Dx_4 + [F_R(-v_0) - F_R(v_{r2})]/c_2, \end{aligned}\right\} \tag{11}$$

with

$$\left.\begin{aligned} (*)' = \mathrm{d}(*)/\mathrm{d}\tau, \quad \tau = \omega_2 t, \quad \omega_2 = \sqrt{(c_2/m_2)}, \\ \gamma = m_1/m_2, \quad \kappa = c_1/c_2, \quad \delta = \mathrm{d}_1/\mathrm{d}_2, \\ D = d_2/2\sqrt{(c_2 m_2)}, \quad v_{r1} = \omega_2 x_2 - v_0, \quad v_{r2} = \omega_2 x_4 - v_0. \end{aligned}\right\} \tag{12}$$

The meaning of the parameters becomes clear from figure 7*b*. Here, the parameter values and initial conditions are, if not specified otherwise: $v_0 = 1$ m s^{-1}, $F_{N1}/c_2 = F_{N2}/c_2 = 20.0$ m, $\omega_2 = 1.0$ rad s^{-1}, and $x_1(0) = x_3(0) = 0$, $x_2(0) = x_4(0) = 1.0$ m s^{-1}, respectively.

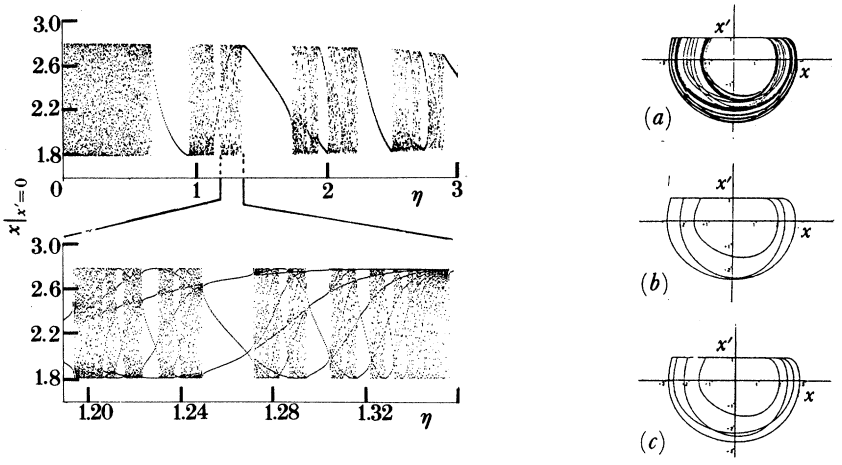

Figure 8. Bifurcation diagram for model A depending on the frequency ratio η with an enlargement and phase-plane plots for (*a*) $\eta = 1.22$, (*b*) $\eta = 1.26$ and (*c*) $\eta = 1.30$, by Jahnke in 1987.

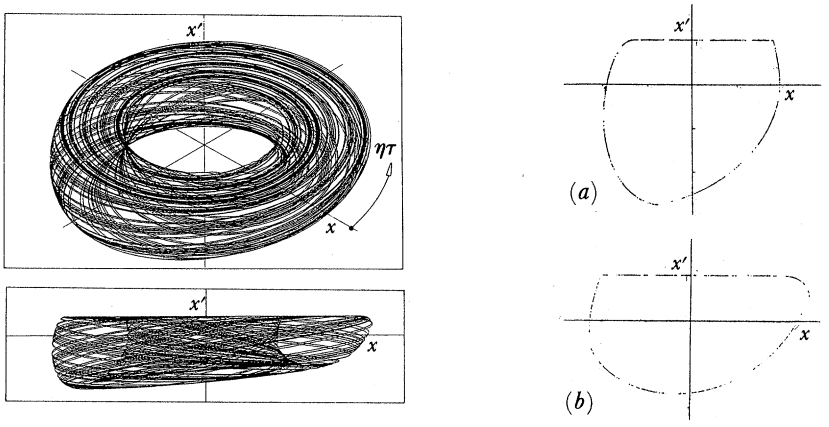

Figure 9. Chaotic motion for model A in the three-dimensional phase space with Poincaré sections, (*a*) $\eta\tau = \frac{5}{4}\pi$ and (*b*) $\eta\tau = \frac{1}{4}\pi$, by Jahnke in 1987.

As an alternative to the state space description the mapping approach will be mentioned. For the system model A and the friction model I, the equations (1)–(4) hold, when the disturbance, $u(t) = u_0 \cos \Omega t$, is regarded in the spring force F_s, i.e. $F_s = c(x - u_0 \cos \Omega t)$. For the slip mode with $v_r < 0$ the solution reads in contrast to equation (6),

$$x(t) = x_s + C \cos(\omega_0 t - \varphi) + V u_0 \cos \Omega t, \tag{13}$$

$$x_s = \mu F_N / c, \quad V = 1/(1-\eta^2), \quad \eta^2 = \Omega^2/\omega_0^2, \quad \omega_0^2 = c/m. \tag{14}$$

For the stick mode, it follows from (3), (4), using the modified spring force ($x_B \leqslant x \leqslant x_A$, $-x_0 \leqslant x_B$):

$$|x - u_0 \cos \Omega t| \leqslant \mu_0 F_N / c \equiv x_0, \tag{15}$$

$$x_A = x(t_A) = x_0 + u_0 \cos \Omega t_A, \tag{16}$$

$$x_A - x_B = v_0 (t_A - t_B). \tag{17}$$

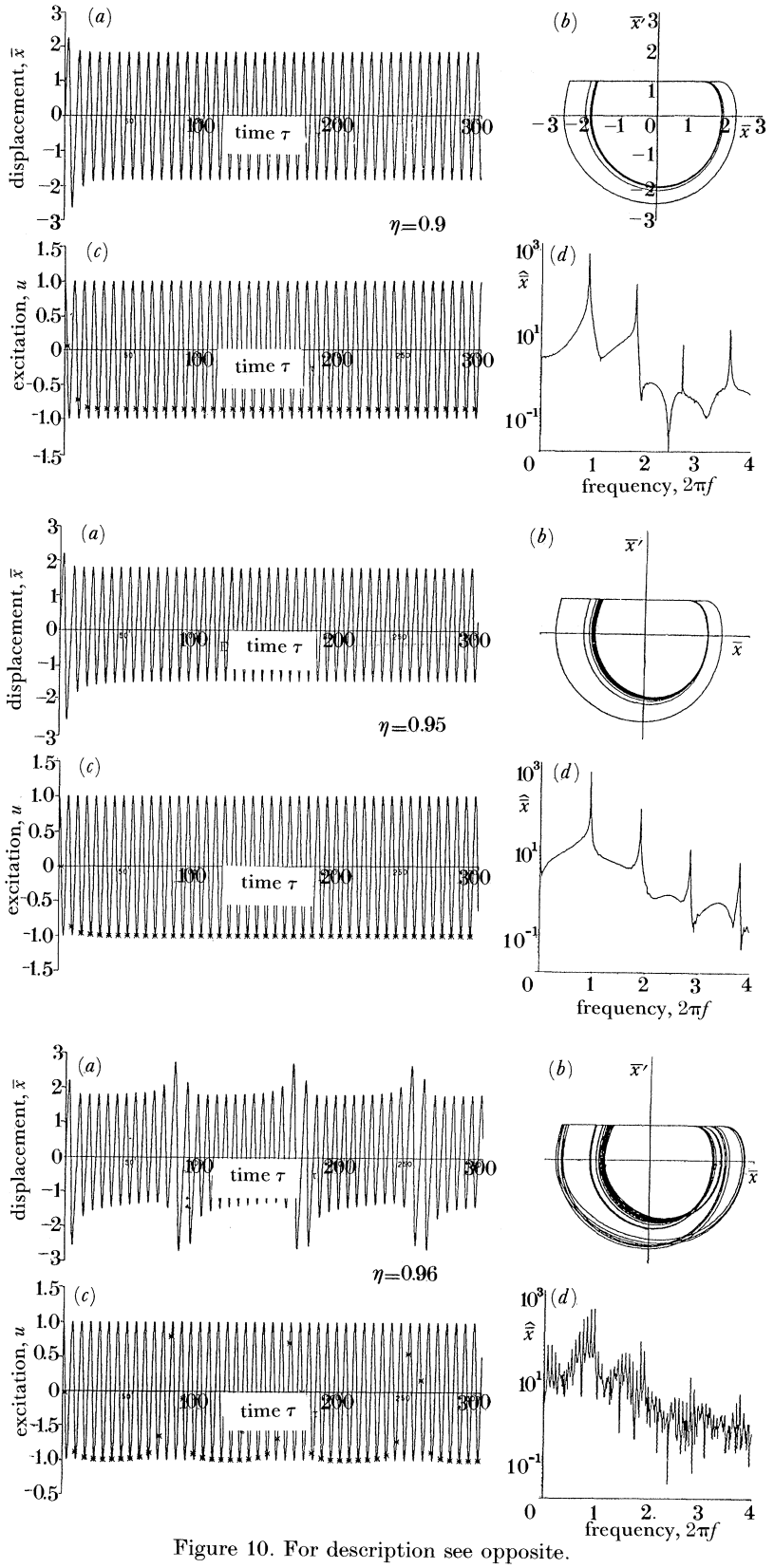

Figure 10. For description see opposite.

PHILOSOPHICAL TRANSACTIONS OF THE ROYAL SOCIETY A MATHEMATICAL, PHYSICAL & ENGINEERING SCIENCES

The disturbance $u(t)$ affects the slip mode as well as the stick mode, cf. (13), (16). But, for $u_0 \ll x_A - x_s$, $u_0 \ll v_0/\omega_0$, the influence on the slip mode may be neglected, resulting in the approximation, cf. figure 4,

$$x_B - x_s = -(x_A - x_s), \quad \omega_0(t_B - t_A) = \pi + 2\varphi, \quad \tan\varphi = v_0/\omega_0(x_A - x_s). \tag{18}$$

Considering successive cycles, equations (16) to (18) yield after eliminating x_B and t_B,

$$\left.\begin{aligned} X_{j+1} + X_j &= \tau_{j+1} - \tau_j - \pi - 2\varphi_j, \quad \tan\varphi_j = 1/X_j, \\ X_{j+1} &= X_0 + U_0 \cos\eta\tau_{j+1}, \end{aligned}\right\} \tag{19}$$

where the following abbreviations were used,

$$X = (x_A - x_s)\,\omega_0/v_0, \quad X_0 = (x_0 - x_s)\,\omega_0/v_0, \quad U_0 = u_0\,\omega_0/v_0, \quad \tau = \omega_0 t_A. \tag{20}$$

In the limit cases $\tan\varphi \ll 1$ and $1/\tan\varphi \ll 1$, further simplifications are possible. From (19) it can be seen, that the equations are invariant if the term $\eta\tau$ is replaced by $\eta\tau + 2k\pi$, where $k = \pm 1, \pm 2, \ldots$, and that the solution is bounded by

$$X_0 - U_0 \leqslant X \leqslant X_0 + U_0. \tag{21}$$

Both properties are useful for finding solutions (cf. Guckenheimer & Holmes 1983), which will not be pursued here.

4. Numerical results of the discrete models

Both discrete models A and B are of order three and four, respectively. Thus they are sufficiently complex to exhibit chaotic behaviour, which will be shown by numerical simulations. The simulation results have been visualized by means of time histories, phase-plane plots, Poincaré-maps and frequency spectra, while bifurcation diagrams show the parameter dependencies. Because of lack of space only some results will be shown in this paper.

The results for model A are given in figures 8, and 9. Figure 8 shows the bifurcation diagram depending on the frequency ratio η together with some selected phase-plane plots. Chaos occurs in certain frequency bands which are separated by bands with p-periodic solutions of order $p = 1$ up to 6. Figure 9 shows the chaotic solution for $\eta = 2.1625$ in the three-dimensional state space as well as two Poincaré sections ($x_3 = \frac{1}{4}\pi$ and $x_3 = \frac{5}{4}\pi$) which exhibit a Cantor-set-like structure. Obviously, the stick mode captures the periodic motions as well as the chaotic ones. Thus, in the present case, all phase-plane plots are bounded by a line $x' = v_0/\omega_0 = \text{const}$. Further, figure 10 shows that the transition into chaos in the frequency range $0.9 \leqslant \eta \leqslant 0.96$ is similar to the intermittency route described by Pomeau & Manneville (1980). Here, the asterisks characterize the transition from the stick to the slip mode. With an increasing frequency ratio η the transition point moves to the lower bound, cf. (21). When the bound is reached, bursts occur in the displacement amplitudes and a chaotic motion is starting.

The results for model B are presented in figures 11, 12 and 13. Figure 11 shows the bifurcation diagram for both masses depending on the damping ratio D ($\kappa = 2.0$, $\gamma = 2.5$, $\delta = 1.0$). The transition to chaos occurs for $0.07 \geqslant D \geqslant 0.04$.

Figure 10. Route to chaos for model A in the frequency range $0,90 \leqslant \eta \leqslant 0,96$: (*a*) time history of displacement, (*b*) phase-plane plot, (*c*) time history of the excitation with points of transition from stick to slip mode, (*d*) frequency spectra, by Jahnke in 1987.

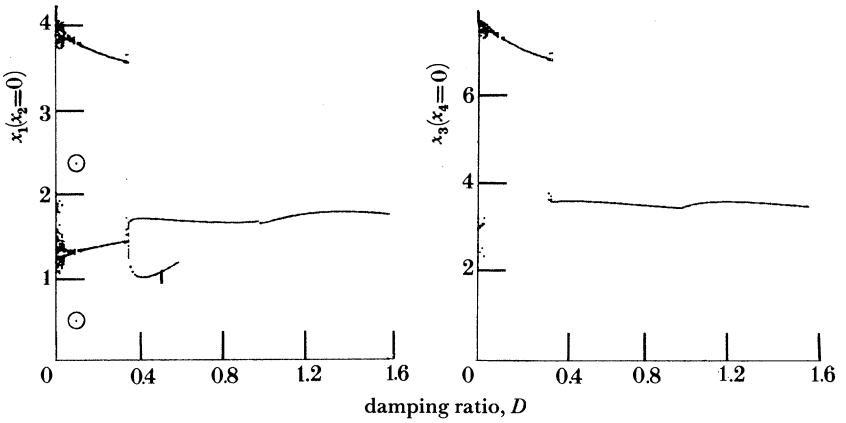

Figure 11. Bifurcation diagrams for model B depending on the damping ratio D, by Wasmann in 1988.

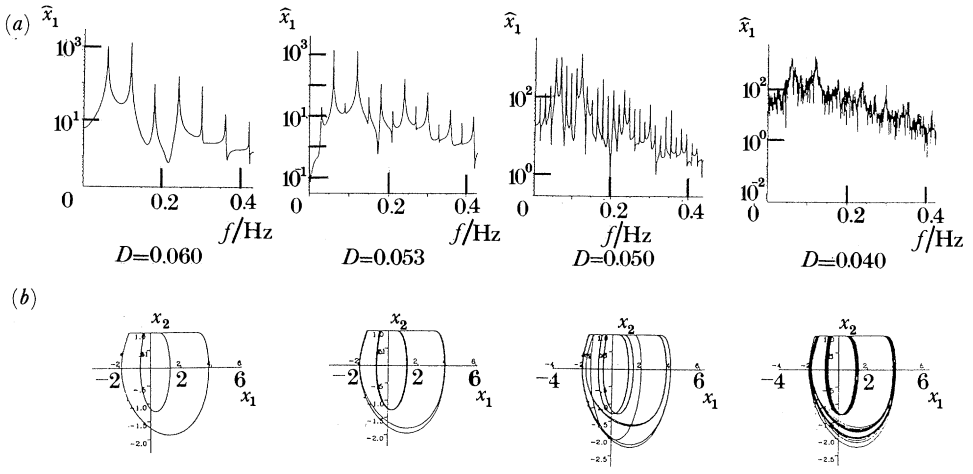

Figure 12. Route to chaos for model B in the damping range $0.060 \geqslant D \geqslant 0.040$: (*a*) frequency spectra, (*b*) phase-plane plots, by Wasmann in 1988.

The corresponding phase-plane plots and frequency spectra for mass 1 reveal, see figure 12, that with decreasing damping the number p of p-periodic solutions increase in the manner $p = 1, 2, 4$. However, for $D = 0.05$ this sequence is interrupted by a $p = 9$ solution. In contrast to model A, chaos is approached similar to the well-known period-doubling route. For high damping, $D > 0.07$, only $p = 1$ solutions occur. Beyond critical damping $D = 1$, only mass 2 performs stick–slip vibrations, while mass 1 remains in a pure slip mode, cf. figure 13.

5. Experimental results of the continuous models

In case of the cantilever beam C, and for the thin plate D, the deflection $z(t)$ has been measured by means of a laser interferometer near the band contact, cf. figure 14. The signals have been processed to gain time histories, phase-plane plots,

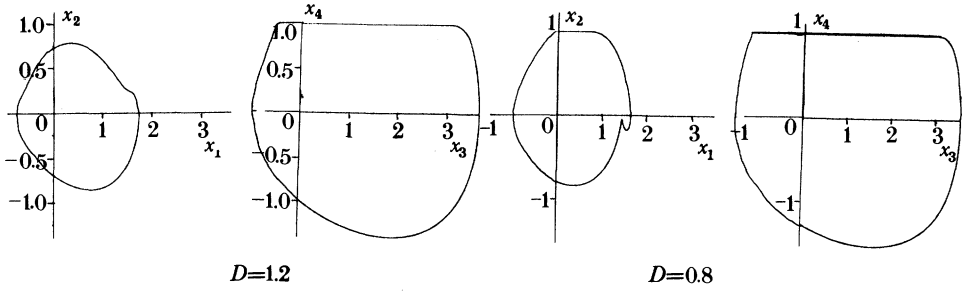

Figure 13. Suppression of the stick mode of mass 1 in model B with increasing damping, by Wasmann in 1988.

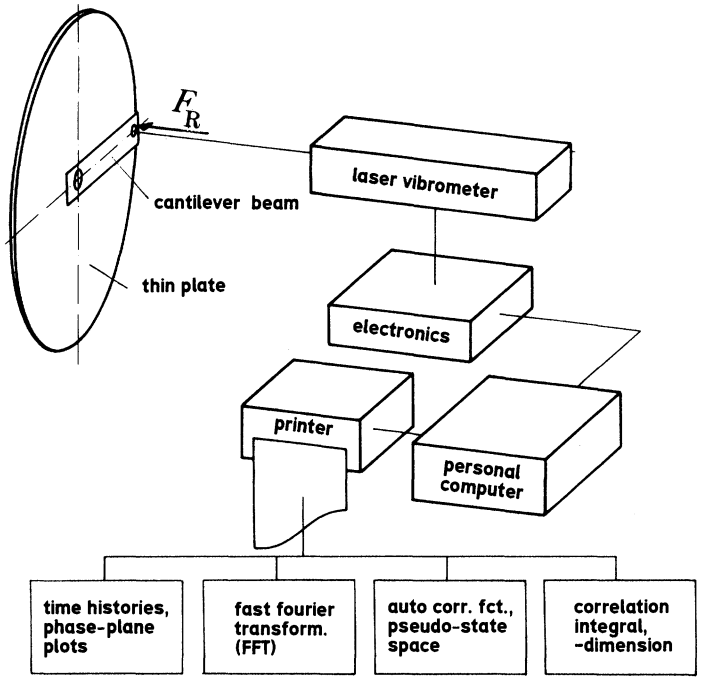

Figure 14. Test set-up for measuring regular and chaotic motions for model C and D using a laser interferometer.

frequency spectra, the autocorrelation function, a pseudo-state space, correlation integrals and the correlation dimension. According to Packard *et al.* (1980), from a single time series of a state variable $z(t)$ a pseudo-state space,

$$\boldsymbol{z}^{\mathrm{T}} = [z(t_0)\, z(t_0+T) \ldots z(t_0+kT)], \quad k = 1(1)\, m-1, \tag{22}$$

can be reconstructed, where m denotes the embedding dimension and T the time delay. Then, following Grassberger & Procaccia (1983), the correlation integral, $C(r) \sim r^{\nu}$, can be found. Here, r denotes the radius of a hypersphere in the pseudo-state space and ν the correlation exponent which depends on the embedding dimension m.

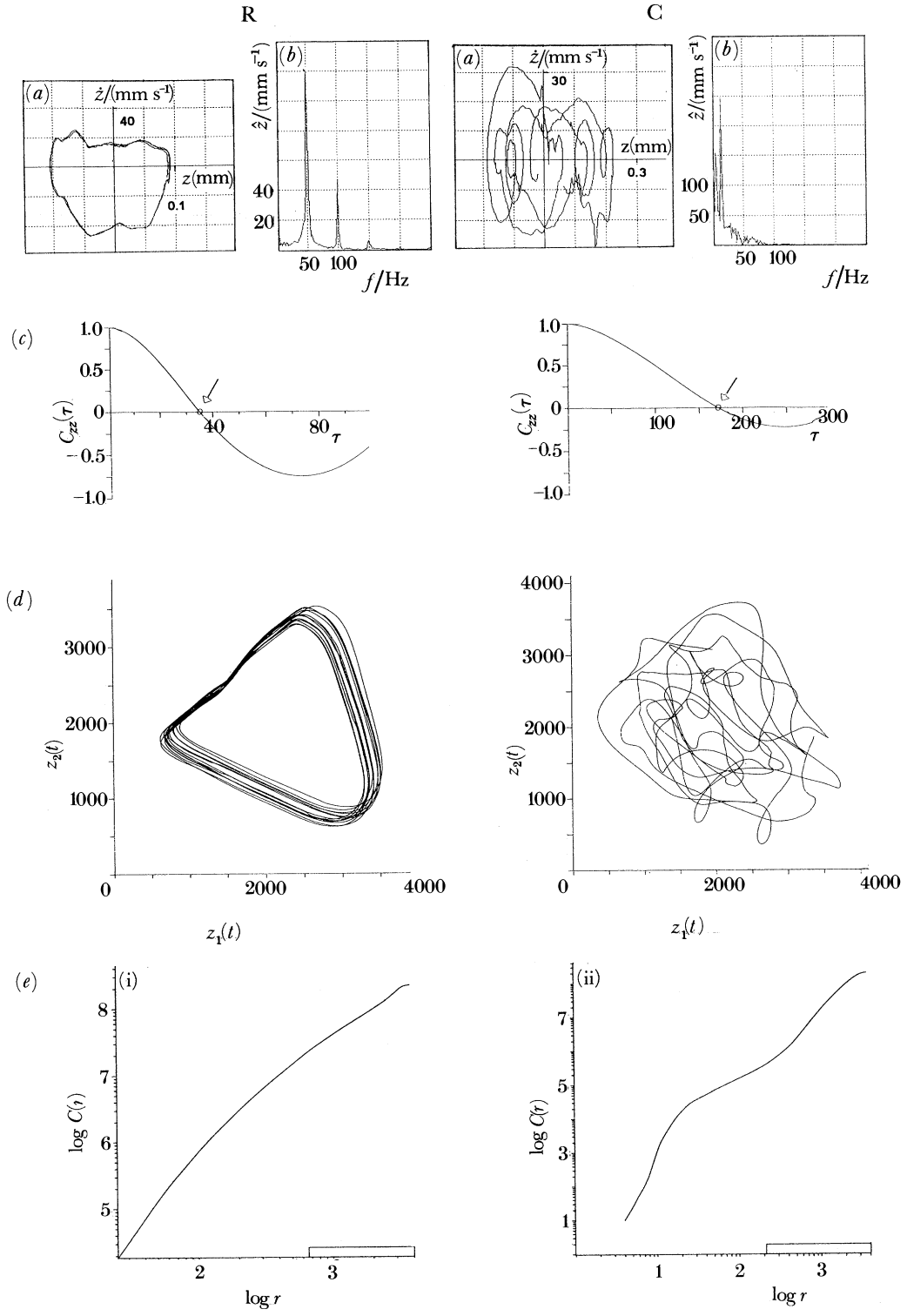

Figure 15. For description see opposite.

PHILOSOPHICAL TRANSACTIONS OF THE ROYAL SOCIETY A MATHEMATICAL, PHYSICAL & ENGINEERING SCIENCES

For sufficient large values of m and a decreasing radius r, the correlation exponent tends to the correlation dimension D_c for a regular or chaotic attractor, while $C(r) \sim r^m$ holds for a pure random noise signal. For a noise signal on top of a deterministic signal, the plot $\log C(r)$ against $\log r$ has two regions. If the noise level is greater than r, then the slope will increase with m, $C(r) \sim r^m$, and if the noise level is less than r, the slope will be constant, $C(r) \sim r^{D_c}$. Therefore, it is possible to distinguish between chaotic and stochastic behaviour of measured signals. On the other hand, the correlation dimension D_c gives a hint to the state space dimension required to model a system which exhibits chaotic behaviour. Figure 15 shows the measured data, the reconstructed time series, the corresponding autocorrelation function and the correlation integral for the cantilever beam, model C. To get linear independent state vectors, the time delay T is taken as the time for the first zero of the corresponding autocorrelation function. Figure 15 R includes the results for a regular motion, and figure 15 C those for a chaotic motion. A comparison of the correlation integrals shows, that in the chaotic case the slope in the $\log C$ against $\log r$ diagram deviates considerably from a straight line. This may indicate the special structure of a chaotic attractor for stick–slip motions, cf. figure 9. However, this phenomenon deserves further investigations.

6. Concluding remarks

Stick–slip vibrations are friction induced self-sustained oscillations. They occur in many engineering systems but also in bowed music instruments. For a violin as an example the excitation mechanism has been explained by means of a simple model of order two. Since realistic models for engineering systems or even for bowed instruments are very complicated, four model problems have been studied. Here, chaotic motions have been found numerically and experimentally. Numerical simulations for two discrete models of order three and four, respectively, resulted in p-periodic solutions of nearly any period up to $p = 9$ as well as in chaotic motions. In the case of a single-degree-of-freedom oscillator with an external harmonic excitation, the routes to chaos are similar to intermittency and all motions showed stick and slip modes. In the case of the two-degree-of-freedom spring-mass-damper-system, the routes into chaos have been found similar to the period-doubling. Here, for certain parameters one mass showed stick–slip motion, while the other remained in a pure slip mode. Experiments performed with a cantilever beam and a thin plate showed also regular or chaotic behaviour, depending on the system parameters. In both cases the friction forces were applied by means of a continuous belt acting on the structure. For the cantilever beam, a pseudo-state space was reconstructed from a time series measured by means of a laser interferometer, utilizing the time delay method. From the behaviour of the correlation integral, the correlation dimension has been obtained for regular and chaotic motions. This scalar quantity describes the dimension of the attractor and, thus, gives information about the order of the system required in an adequate model.

Figure 15. Experimental results for model C (cantilever beam): regular behaviour (R), chaotic behaviour (C), (*a*) measured phase-plane plots, (*b*) frequency spectra, (*c*) autocorrelation functions, (*d*) relation of the first two variables in the pseudo-state space, (*e*) correlation integrals $C(r)$. (*e*) (i) $F_N = 35$ N, $v_0 = 1.4$ cm s^{-1}, $D_c = 1.5$, $m = 3$; (ii) $F_N = 85$ N, $v_0 = 14.3$ cm s^{-1}, $D_c = 1.9$, $m = 4$.

This research was financed by the Volkswagen foundation under the contract no. I/63177. The authors acknowledge gratefully this support and also like to thank their former students M. Jahnke and U. Wasmann, who have contributed to this research by their project work.

References

Abraham, R. H. & Shaw, C. D. 1983–88 *Dynamics – the geometry of behaviour*. Santa Cruz: Aerial Press.

Bishop, R. E. D. 1965 *Vibrations*. Cambridge University Press.

Bochet, B. 1961 Nouvelles Recherches Experimentelles sur le Frottement et Glissement. *Annls Mines Carbur.* **19**, 27–120.

Conti, P. 1875 Sulla Resistanza die Attrito. *Accrd. Lincei* **11** (16).

Cremer, L. 1981 *Physik der Geige*. Stuttgart: Hirzel.

Fingberg, U. 1989 A wheel-rail-squealing-noise model. *Proc. Polish–German Workshop on Dyn. Problems in Mech. Syst., Madralin, Poland* (ed. R. Bogacz & K. Popp), pp. 111–222. Warsaw: Polska Akademia Nauk.

Franke, J. 1882 Über die Abhängigkeit der gleitenden Reibung von der Geschwindigkeit. Civil-Ing.

Galton, G. 1878 The action of brakes. On the effect of brakes upon railway trains. *Engng* **25**, 469–472.

Grabec, I. 1988 Explanation of random vibrations in cutting on grounds of deterministic chaos. *Robotics Computer-Integrated Manufacturing*, **4**, 129–134.

Grassberger, P. & Procaccia, I. 1983 Measuring the strangeness of strange attractors. *Physica* D **9**, 189–208.

Guckenheimer, J. & Holmes, P. 1983 *Nonlinear oscillations, dynamical systems, and bifurcations of vector fields*. New York: Springer.

Hendriks, F. 1983 Bounce and chaotic motion in impact print hammers. *IBM J. Res. Development* **27** (3), 24–31.

Helmholtz, H. v. 1913 Lehre von den Tonempfindungen, 6th edn. Braunschweig.

Hsu, C. S. 1987 *Cell-to-cell mapping*. New York: Springer.

Kaas-Petersen, C. & True, H. 1985 Periodic, biperiodic and chaotic dynamical behaviour of railway vehicles. *Proc. 9th IAVSD Symp. Linkoping*, pp. 208–221.

Kunick, A. & Steeb, W.-H. 1986 *Chaos in dynamischen Systemen*. Mannheim: BI.

Magnus, K. 1961 *Schwingungen*. Stuttgart: Teubner.

McIntyre, M. E. & Woodhouse, J. 1979 *Acoustica* **43**, 93.

Moon, F. C. & Shaw, S. W. 1983 Chaotic vibrations of a beam with non-linear boundary conditions. *Int. J. Non-Linear Mech.* **18**, 465–477.

Neimark, Ju. J. & Landa, P. S. 1987 *Stochastic and chaotic vibrations*. Moscow: Nauka. (In Russian).

Packard, N. H., Crutchfield, J. P., Farmer, J. D. & Shaw, R. S. 1980 Geometry of time series. *Phys. Rev. Lett.* **45**, 712–716.

Paidoussis, M. P. & Moon, F. C. 1988 Nonlinear and chaotic fluidelastic vibrations of a flexible pipe conveying fluid. *J. Fluids Structures* **2**, 567–591.

Pfeiffer, F. 1988 Seltsame Attraktoren in Zahnradgetrieben. *Ing. Arch.* **58**, 113–125.

Pomeau, Y. & Manneville, P. 1980 Intermittent transition to turbulence in dissipative dynamical systems. *Communs math. Phys.* **74**, 189–197.

Popp, K., Schneider, E. & Irretier, H. 1985 Noise generation in railway wheels due to rail-wheel contact forces. *Proc. 9th IAVSD Symp., Linkoping*, pp. 448–466.

Popp, K. & Stelter, P. 1990 Nonlinear oscillations of structures induced by dry friction. *Proc. IUTAM Symp. on Nonlin. Dyn. in Engineering Systems, Stuttgart* (ed. W. Schiehlen), pp. 233–240.

Skalmierski, B. 1981 The construction of old Italian violins: tentative explanation. *Bull. Acad. Polonaise Sci.* (*techniques*) **29**, 175–181.

Stelter, P. & Popp, K. 1989 Chaotic behaviour of structures excited by dry friction forces. *Proc. Workshop on Rolling Noise Generation, Berlin* (ed. M. Heckl), pp. 102–111.

Szczygielski, W. M. 1986 Dynamisches Verhalten eines schnell drehenden Rotors bei Anstreifvorgängen. Diss. ETH Zürich Nr. 8094.

Thompson, J. M. T. & Stewart, H. B. 1986 *Nonlinear dynamics and chaos*. Chichester: Wiley.

Utkin, V. I. 1978 *Sliding modes and their application in variable structure systems* (Engl. Transl.). Moscow: MIR Publ.

PHILOSOPHICAL TRANSACTIONS OF THE ROYAL SOCIETY A MATHEMATICAL, PHYSICAL & ENGINEERING SCIENCES